Electronic Supporting Information

Exfoliation of large-flake, few-layer MoS_2 nanosheets mediated by carbon nanotubes

Wenqian Han,[a] Yan Xia,[b] Dong Yang*[b] and Angang Dong*[a]

[a]*Shanghai Key Laboratory of Molecular Catalysis and Innovative Materials and Department of Chemistry, Fudan University, Shanghai 200433, China.*

[b]*State Key Laboratory of Molecular Engineering of Polymers and Department of Macromolecular Science, Fudan University, Shanghai 200433, China.*

Experimental Section

Chemicals. Bulk MoS_2 powder, bulk WS_2 powder, ammonium tetrathiotungstate ($(NH_4)_2MoS_4$, 99.9%), and Nafion (5 wt%) were purchased from Sigma-Aldrich. Carbon nanotubes powder (CNTs, 20 nm in diameter) and graphite powder were purchased from Qingdao Haoxin Co. Ltd (China). Sodium 2-naphthalenesulfonate (SNS, 85%) was purchased from Aladdin. All chemicals were used as received without further purification.

Preparation of CNT dispersions. 4 g of CNT powder and 1 g of SNS were mixed in 995 g of ethanol. The resulting mixture was then sonicated for 30 min to obtain a homogeneous CNT dispersion (0.4 wt%).

Exfoliation of MoS_2 nanosheets. Both commercial and home-made MoS_2 crystals can be used as precursors for preparing large-flake MoS_2 nanosheets, although home-made MoS_2 may give rise to a higher exfoliation efficiency. Home-made bulk MoS_2

crystals were synthesized by heating 10 g of $(NH_4)_2MoS_4$ at 450 ºC under Ar/H_2 (95%:5% by volume) for 2 h. To prepare exfoliated MoS_2 nanosheets, commercial MoS_2 powder (5 g) or home-made MoS_2 crystals was added into 500 g of the above prepared CNT dispersion in a flask. The resulting mixture was then subjected to sonication using a benchtop sonicator (Derui M07, 80 W), resulting in a black suspension after 30 min. To remove CNTs, the exfoliation mixture was heated at 50 °C for 15 min, inducing the sedimentation of CNTs. The yellowish supernatant was collected by centrifugation for further use. The supernatant containing MoS_2 nanosheets and residual CNTs was allowed to evaporate at 60 °C for 30 min to obtain a solid powder, which could be directly used for preparing working electrodes for subsequent electrochemical applications. The exfoliation of WS_2 and graphene nanosheets was carried out by replacing bulk MoS_2 with bulk WS_2 and graphite while keeping other exfoliation conditions constant.

Characterization. Transmission electron microscopy (TEM) and high-resolution TEM (HRTEM) were obtained on a Tecnai G2 F20 S-Twin microscope operated at 200 kV. Aberration-corrected high-angle annular dark-field scanning TEM (HAADF-STEM) was carried out on a JEM-ARM200F microscope operated at 200 kV. Scanning electron microscopy (SEM) was conducted on a Zeiss Ultra-55 microscope operated at 5 kV. Powder X-ray diffraction (XRD) was performed on a Bruker D4 X-ray diffractometer (40 kV, 40 mA). X-ray photoelectron spectroscopy (XPS) was conducted on a Perkin Elmer PHI-5000C ESCA system. Raman measurements were obtained on an XploRA Raman system. Nitrogen adsorption-desorption isotherms were obtained on

an ASAP 2020 system. All samples were degassed under vacuum at 180 °C for at least 8 h prior to measurement. The pore size distributions were derived from the adsorption branch of the isotherms using the Barrett-Joyner-Halenda (BJH) model. Thermogravimetric analysis (TGA) was carried out on a Perkin-Elmer Pyris 1 thermogravimetric analyzer. Fourier-transform infrared (FTIR) spectra were acquired using a PerkinElmer Spectrum Two spectrometer. AFM was carried out on a Bruker Fastscan AFM instrument in the tapping mode. The sample was made by dropping the exfoliated MoS_2 nanosheet ethanol dispersion on a clean SiO_2/Si substrate followed by drying in air.

Electrochemical tests (HER). All electrochemical measurements were carried out on an AutoLab 204N (Metrohm) electrochemical workstation with a three-electrode system in 0.5 M H_2SO_4. A saturated calomel electrode (SCE), a graphitic rod and a glassy carbon electrode (GCE) with a diameter of 3 mm were used as reference electrode, counter electrode and working electrode, respectively. MoS_2 nanosheets (1 mg) and nafion (5 wt%, 6 μL) were dispersed in ethanol (250 μL) and sonicated for at least 40 min to obtain homogeneous inks. Afterwards, the inks were drop-cast onto the glassy carbon electrode followed by drying. Linear sweep voltammetry (LSV) was measured at a scan rate of 10 mV/s. Electrochemical impedance spectroscopy (EIS) was tested in the frequency range of 10^6-10^{-2} Hz. All the electrochemical measurements were calibrated with a reversible hydrogen electrode (RHE). Cyclic voltammograms (CV) were carried out in the potential window of 0.1-0.2 V (vs. RHE) with scan rates

varying from 60 to 100 mV/s and were further used to calculate the double-layer capacitance (C_{dl}).

Electrochemical tests (SIBs). The sodium-storage performance was evaluated using two electrode CR2016 coin-type cells. The working electrodes were prepared by a slurry-coating procedure. The exfoliated MoS_2 nanosheets and polyvinylidene fluoride (PVDF) binder with a mass ratio of 9:1 were dispersed in N-methyl-2-pyrrolidinone (NMP) to prepare a slurry. This slurry was uniformly painted on a copper foil current collector. The electrodes were dried at 90 ℃ under vacuum overnight. The electrolyte was a 1.0 M $NaClO_4$ solution in a volume ratio of 50:50 mixture of ethylene carbonate and ethyl methyl carbonate. And the separator was a glass fibre film (Whatman). Cyclic voltammetry (CV) was measured on a CHI 660E electrochemical workstation. Galvanostatic tests were carried out on a Neware cell test system with a voltage range of 0.01-3 V.

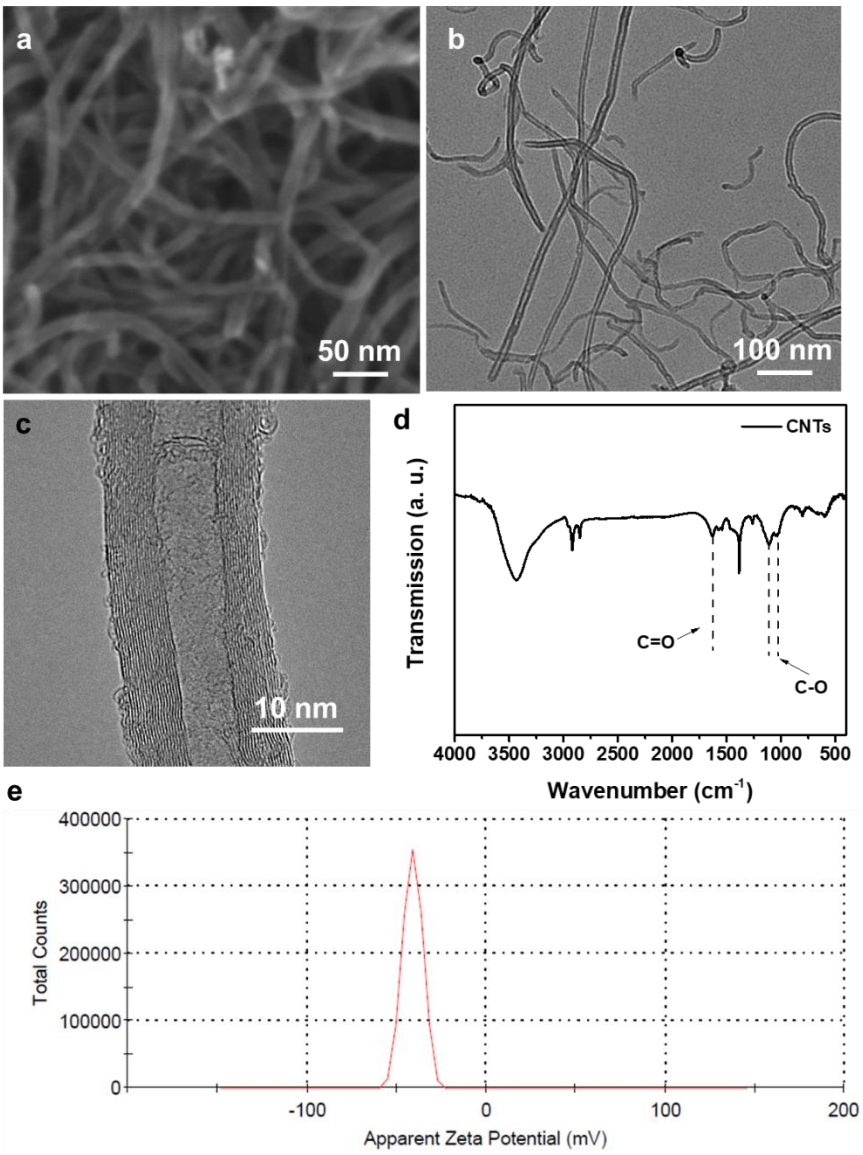

Fig. S1 (a) SEM and (b) TEM images of CNTs with a diameter of ~20 nm, which were used for exfoliating bulk MoS_2. (c) HRTEM image, (d) FTIR spectrum, and (e) zeta potential measurements of CNTs. The characteristic peaks at 1635 cm^{-1} (C=O stretching mode), 1046 cm^{-1}, and 1092 cm^{-1} (C-O stretching modes) in the FTIR spectrum suggest the presence of a certain amount of oxygen-containing functional groups at the CNT surface.

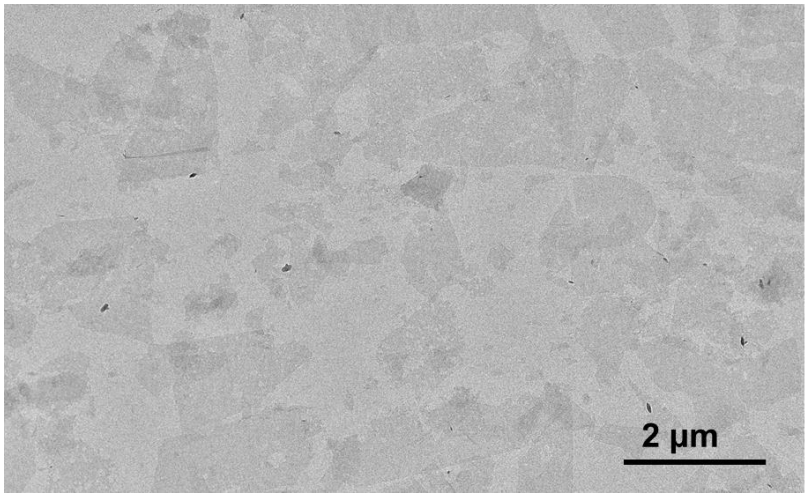

Fig. 2 Low-magnification TEM image of exfoliated large-flake MoS_2 nanosheets.

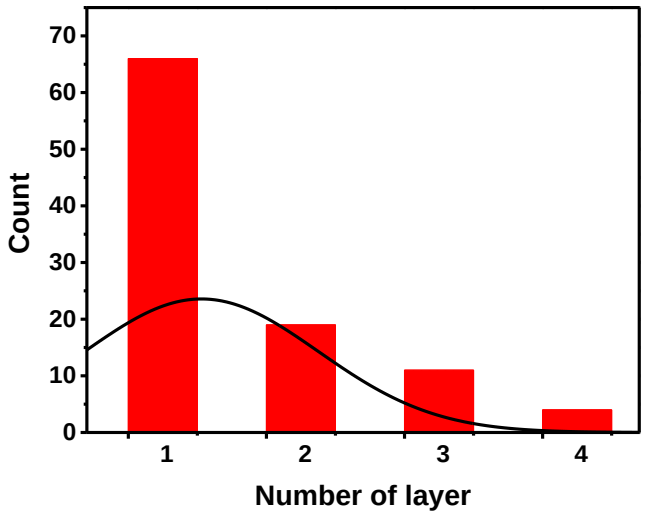

Fig. S3 Layer number distribution histograms of exfoliated MoS_2 nanosheets.

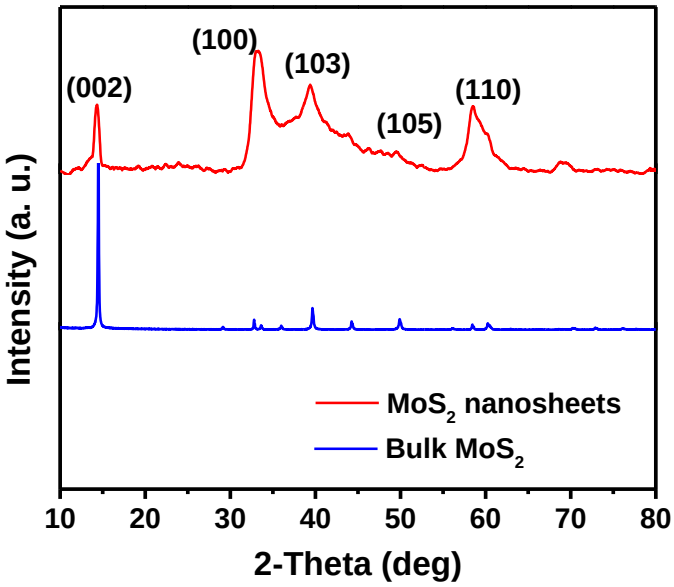

Fig. S4 XRD pattern of MoS_2 nanosheets obtained by exfoliation with SNS only. The XRD pattern of bulk MoS_2 was also added for comparison. The much sharper diffraction peaks compared with few-layer MoS_2 in Fig. 3a indicates that MoS_2 nanosheets obtained by exfoliation with SNS only have thicker layer thickness.

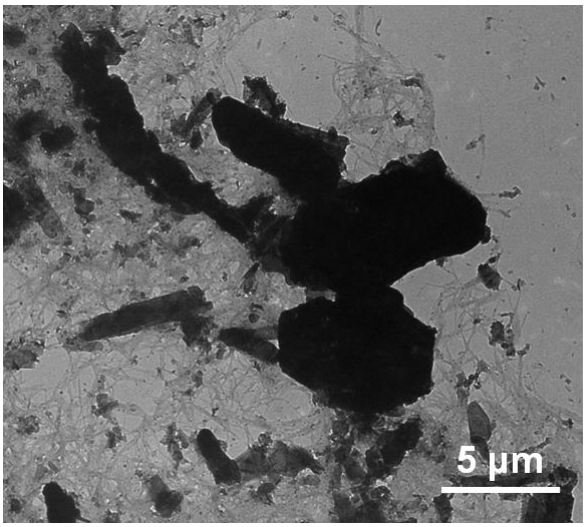

Fig. S5 TEM image of MoS_2 flakes resulting from exfoliation of bulk MoS_2 with CNTs only.

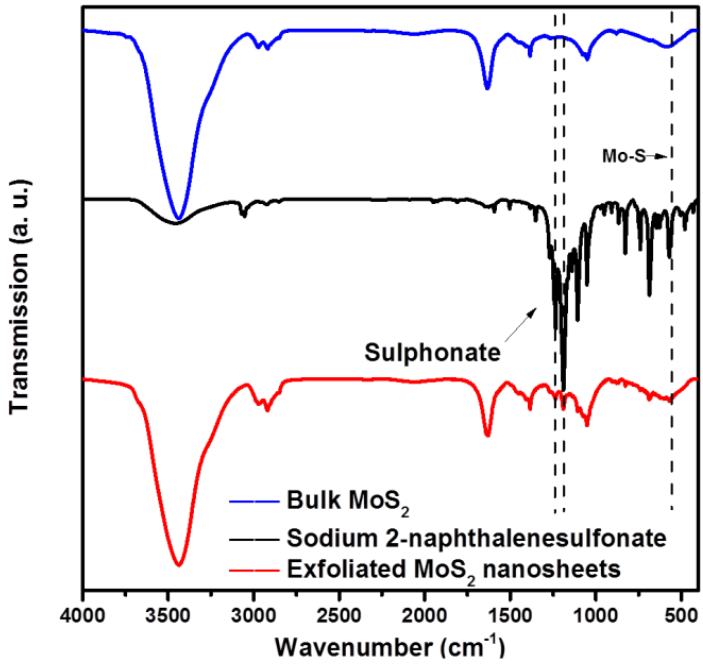

Fig. S6 FTIR spectra of bulk MoS_2, as-exfoliated MoS_2 nanosheets (after 50 °C treatment) and SNS. For MoS_2 nanosheets, the emergence of sulphonate group at 1190 and 1234 cm^{-1} suggests that SNS acts as surfactant to stabilize MoS_2 nanosheets in ethanol.

Fig. S7 Photograph of a MoS_2 nanosheets ethanol dispersion after a week, showing its high colloidal stability.

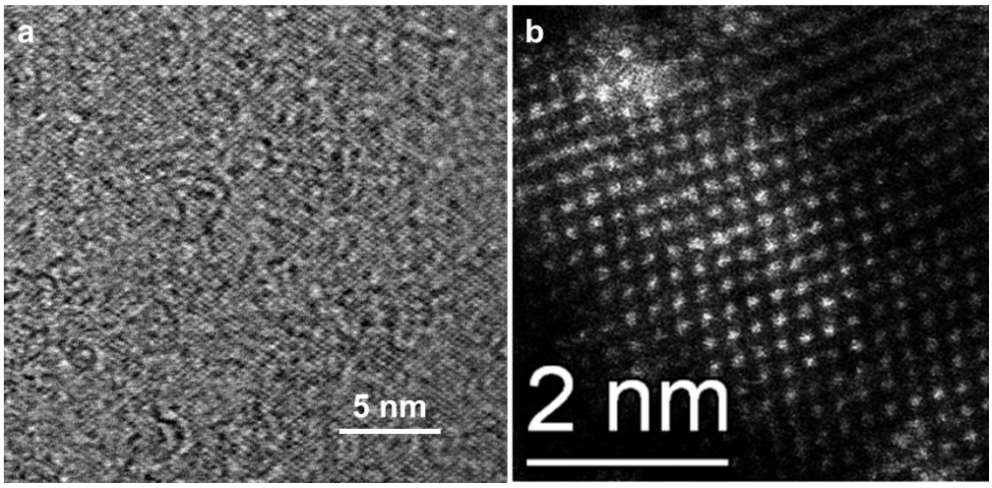

Fig. S8 (a) HRTEM and (b) aberration-corrected HAADF-STEM images of exfoliated MoS_2 nanosheets, showing the high single crystallinity.

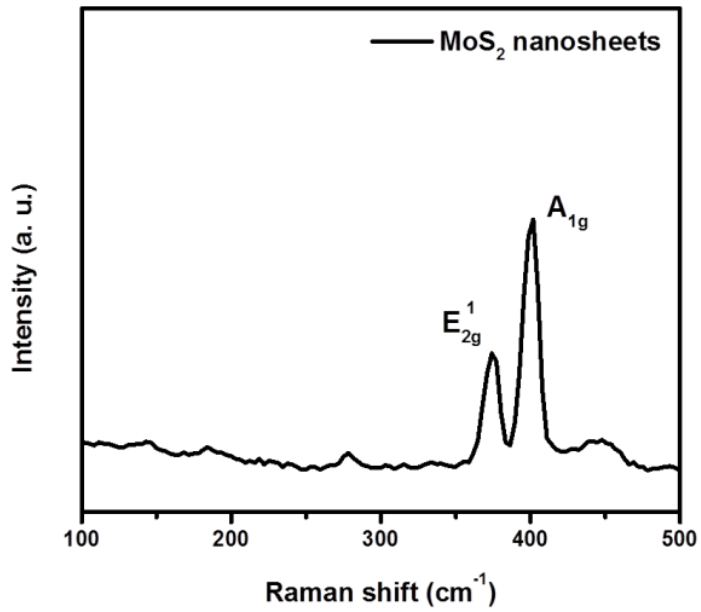

Fig. S9 Raman spectrum of exfoliated MoS_2 nanosheets. The characteristics peaks (J_1-157 cm^{-1}, J_2-226 cm^{-1} and J_3-330 cm^{-1}) ascribed to 1T-phase MoS_2 were not observable, confirming the 2H-phase of exfoliated MoS_2 nanosheets,

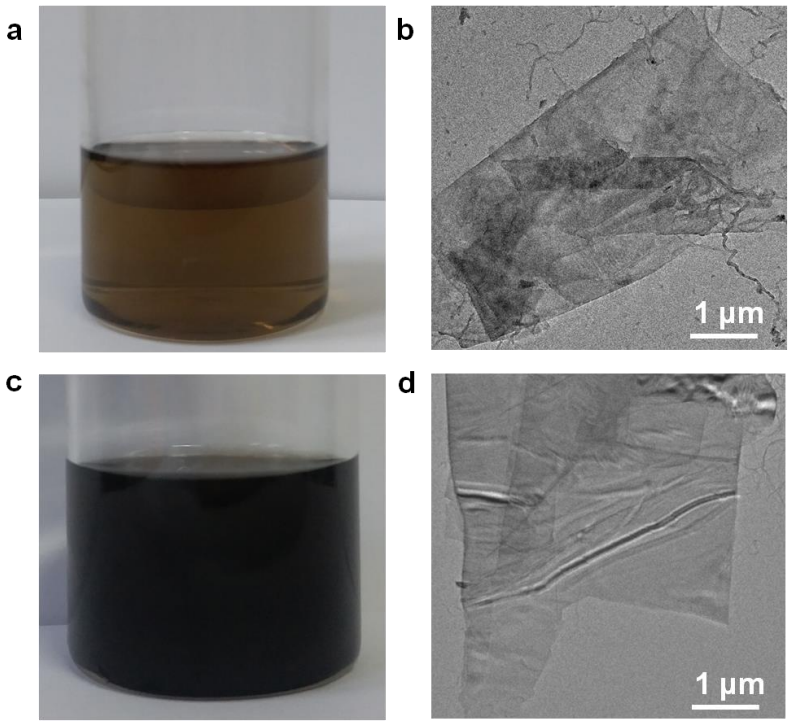

Fig. S10. Photographs and TEM images of (a, b) WS_2 and (c, d) graphene nanosheets obtained by CNT-mediated exfoliation.

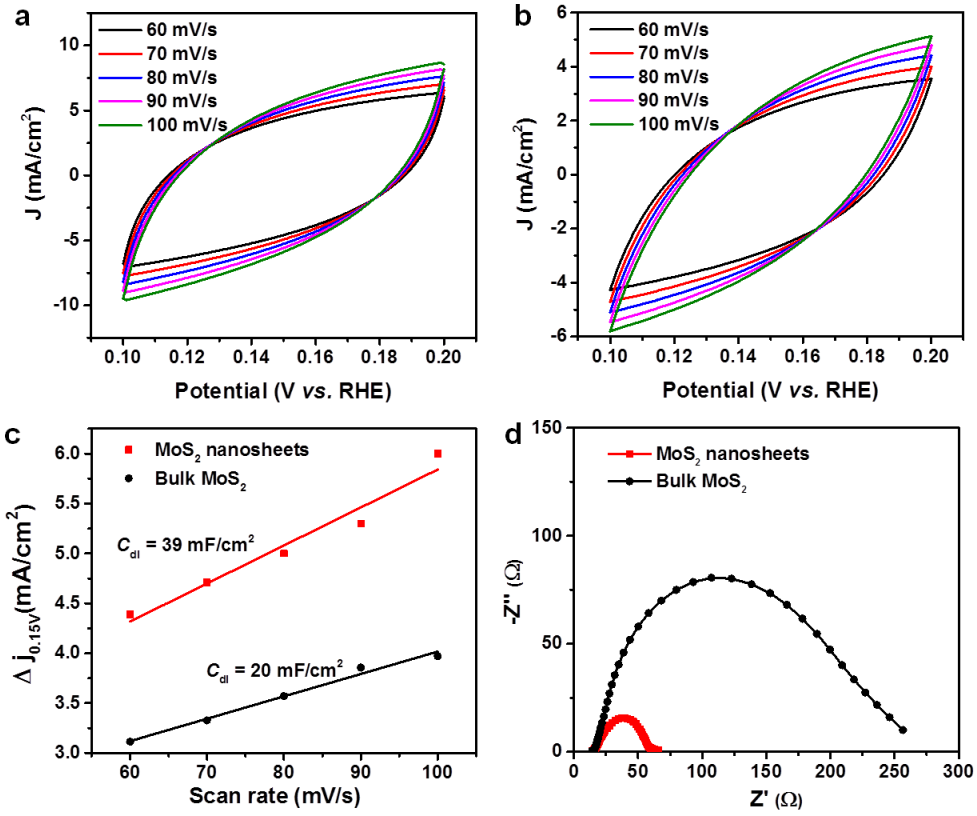

Fig. S11 CV curves of (a) exfoliated MoS_2 nanosheets and (b) bulk MoS_2. (c) Plots of C_{dl} for exfoliated MoS_2 nanosheets and bulk MoS_2. (d) Nyquist plots of exfoliated MoS_2 nanosheets and bulk MoS_2 when evaluated as electrocatalysts for the HER.

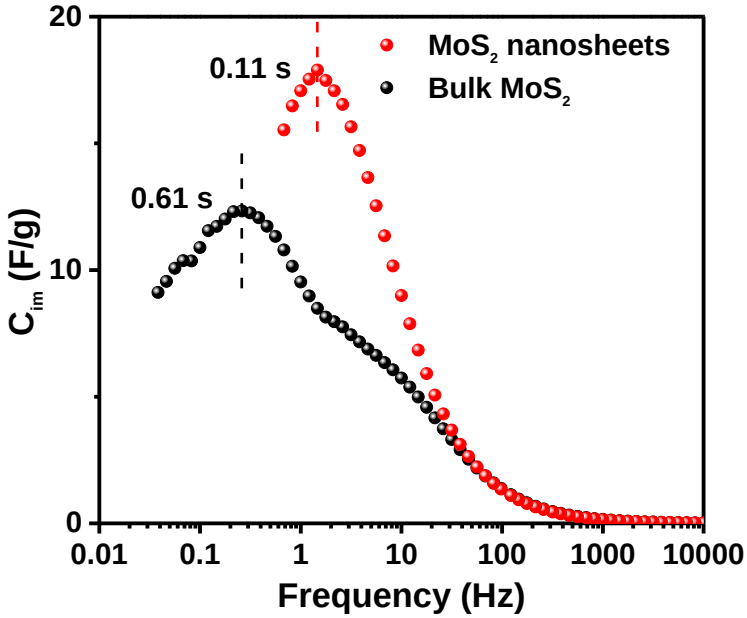

Fig. S12 Imaginary part of complex capacitance (C_{im}) as a function of frequency (f). The relaxation time constant (τ_0) was calculated from the peak frequency using $\tau_0 = (2\pi f)^{-1}$.

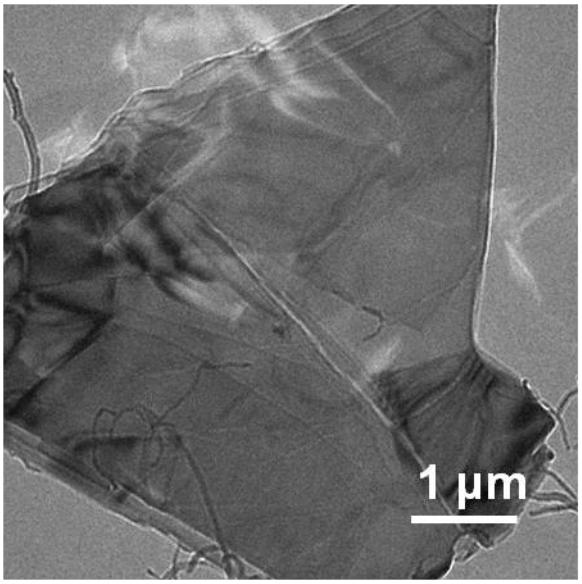

Fig. S13 TEM image of MoS_2 nanosheets after 5000 HER cycles.

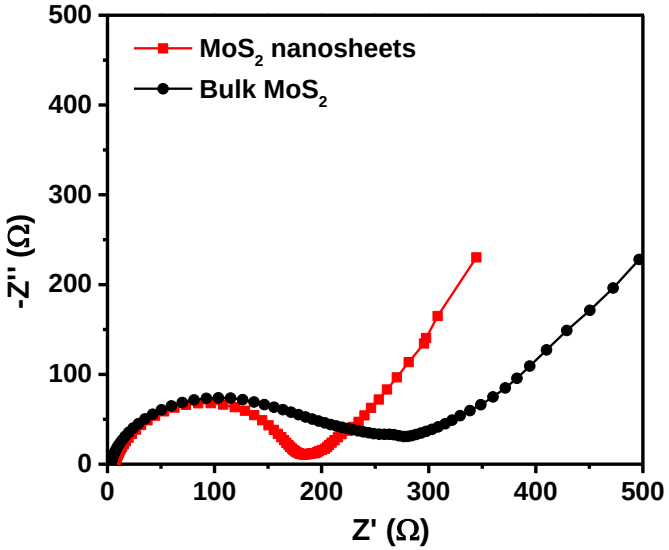

Fig. S14 EIS plots of MoS_2 nanosheets and bulk MoS_2 when evaluated as anodes for SIBs.

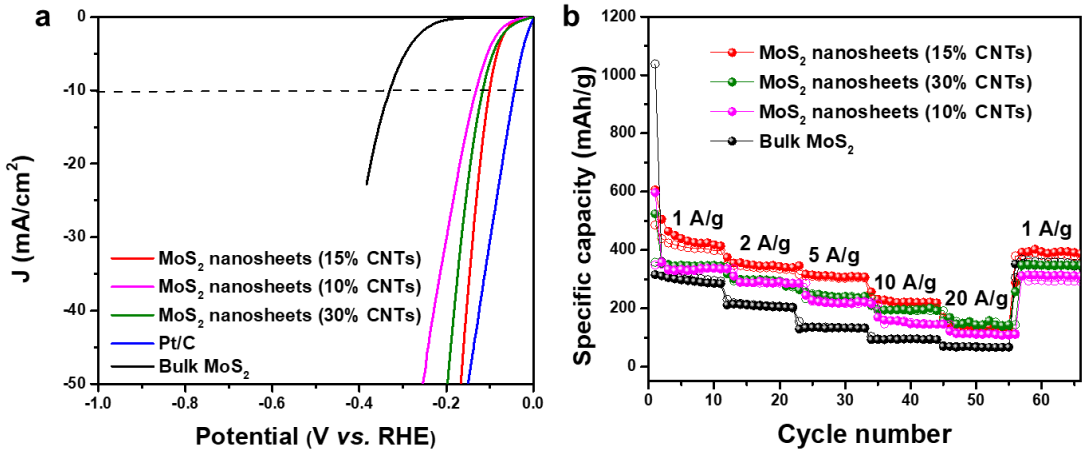

Fig. S15 (a) LSV curves and (b) rate performance of MoS_2 nanosheets with different CNT contents.

The HER activity of 15 wt% and 30 wt% samples are close, which is superior to that of their 10 wt% counterpart, demonstrating that increasing the content of CNTs is important for enhancing the HER activity. Presumably, CNTs not only increase the electrical conductivity, but also prevent the self-stacking of MoS_2 nanosheets, both of which are desirable for boosting the HER. In case of sodium-ion batteries, however, more active materials are desirable in order to achieve a high sodium-storage capacity. Rate-capability measurements show that the rate performance of MoS_2 nanosheets with 30 wt% CNTs is inferior to that of the 15 wt% sample, probably due to the insufficient amount of active materials. Taken together, both HER and SIB results clearly demonstrate that CNTs play a key role in enhancing electrochemical performance, and ~15 wt% of CNTs is an optimal content.

Table S1. Exfoliation yield comparison between our method and other exfoliation methods reported previously.

Exfoliation methods	Solvent	Yield (%)	Ref.
CNTs-mediated exfoliation	Ethanol	45	This work
Liquid exfoliation	NMP	40	[1]
Ethylenediamine-assisted exfoliation	Propylene carbonate	23.2	[2]
n-Butyllithium intercalation exfoliation	Hexanes	11-15	[3]
Aqueous surfactant solutions exfoliation	Deionized water	10	[4]
Shear exfoliation	NMP	4.8	[5]
Shear exfoliation	Deionized water	0.8	[6]

Table S2. HER performance comparison between our exfoliated MoS_2 nanosheets and 2H-MoS_2 catalysts reported previously.

Catalysts	Electrolyte	Overpotential (mV) at 10 mA/cm^2	Tafel slpoe (mV/dec)	Ref.
MoS_2 nanosheets/CNTs	0.5 H_2SO_4	-101	43	This work
Freestanding MoS_2 monolayers	0.5 H_2SO_4	-156	58	[7]
Edge-oriented MoS_2/rGO	0.5 H_2SO_4	-129	43	[8]
Nafion-assisted exfoliated MoS_2	0.5 H_2SO_4	-609	106	[9]
Plasma exfoliated MoS_2	0.5 H_2SO_4	-118	73	[10]
Electrochemically exfoliated MoS_2	0.5 H_2SO_4	-127	199	[11]
Conducting MoS_2 nanosheets	0.5 H_2SO_4	-250	75	[12]
Strained MoS_2 with S-vacancies	0.5 H_2SO_4	-170	60	[13]
MoS_2@graphene	0.5 H_2SO_4	~-230	46	[14]
MoS_2 foams	0.5 H_2SO_4	-156	74	[15]
P-doped 2H-MoS_2	0.5 H_2SO_4	~-225	49	[16]
3D MoS_2 van der Waals heterostructures	0.5 H_2SO_4	-243	82.5	[17]

Table S3. SIB performance comparison between our exfoliated MoS_2 nanosheets and representative state-of-the-art 2H-MoS_2 anode materials reported previously.

Anodes	Voltage range (V)	Current density (A/g)/capacity retention (mAh/g)/cycle number	Ref.
MoS_2 nanosheets/CNTs	0.01-3	2/280/500	This work
Ultrathin MoS_2 nanosheets	0.01-3	0.04/386/100	[18]
Interlayer expanded MoS_2 nanoribbons	0.01-3	5/158/1500	[19]
Ultrathin MoS_2@MOFs	0.01-3	1/265/1000	[20]
Hybrid MoS_2@graphene	0.01-3	0.3/421/250	[21]
Low crystalline MoS_2 nanoflakes	0.01-3	2/337/800	[22]
MoS_2 nanosheets@mesoporous carbon spheres	0.01-3	1/200/300	[23]
Monolayer-rich MoS_2 nanosheets	0.01-3	0.1/385/100	[24]

Reference

1. A. O Neill, U. Khan and J. N. Coleman, *Chem. Mater.*, 2012, **24**, 2414-2421.
2. A. Ghorai, S. K. Ray and A. Midya, *ACS Applied Nano Materials*, 2019, **2**, 1170-1177.
3. X. Fan, P. Xu, Y. C. Li, D. Zhou, Y. Sun, M. A. T. Nguyen, M. Terrones and T. E. Mallouk, *J. Am. Chem. Soc.*, 2016, **138**, 5143-5149.
4. R. J. Smith, P. J. King, M. Lotya, C. Wirtz, U. Khan, S. De, A. O'Neill, G. S. Duesberg, J. C. Grunlan, G. Moriarty, J. Chen, J. Wang, A. I. Minett, V. Nicolosi and J. N. Coleman, *Adv. Mater.*, 2011, **23**, 3944-3948.
5. Y. Li, X. Yin and W. Wu, *Ind. Eng. Chem. Res.*, 2018, **57**, 2838-2846.
6. E. Varrla, C. Backes, K. R. Paton, A. Harvey, Z. Gholamvand, J. McCauley and J. N. Coleman, *Chem. Mater.*, 2015, **27**, 1129-1139.
7. X. Hai, W. Zhou, S. Wang, H. Pang, K. Chang, F. Ichihara and J. Ye, *Nano Energy*, 2017, **39**, 409-417.
8. Y. Sun, F. Alimohammadi, D. Zhang and G. Guo, *Nano Lett.*, 2017, **17**, 1963-1969.
9. N. K. Oh, H. J. Lee, K. Choi, J. Seo, U. Kim, J. Lee, Y. Choi, S. Jung, J. H. Lee, H. S. Shin and H. Park, *Chem. Mater.*, 2018, **30**, 4658-4666.
10. V. Nguyen, P. A. Le, Y. Hsu and K. Wei, *ACS Appl. Mater. Inter.*, 2020, **12**, 11533-11542.
11. X. Pan, M. Yan, C. Sun, K. Zhao, W. Luo, X. Hong, Y. Zhao, L. Xu and L. Mai,

Adv. Funct. Mater., 2020, 2007840.
12. D. Voiry, M. Salehi, R. Silva, T. Fujita, M. Chen, T. Asefa, V. B. Shenoy, G. Eda and M. Chhowalla, *Nano Lett.*, 2013, **13**, 6222-6227.
16. H. Li, C. Tsai, A. L. Koh, L. Cai, A. W. Contryman, A. H. Fragapane, J. Zhao, H. S. Han, H. C. Manoharan, F. Abild-Pedersen, J. K. Nørskov and X. Zheng, *Nat. Mater.*, 2016, **15**, 48-53.
14. Y. Li, J. Wang, X. Tian, L. Ma, C. Dai, C. Yang and Z. Zhou, *Nanoscale*, 2016, **8**, 1676-1683.
15. J. Deng, H. Li, S. Wang, D. Ding, M. Chen, C. Liu, Z. Tian, K. S. Novoselov, C. Ma, D. Deng and X. Bao, *Nat. Commun.*, 2017, **8**, 14430.
16. X. Huang, M. Leng, W. Xiao, M. Li, J. Ding, T. L. Tan, W. S. V. Lee and J. Xue, *Adv. Funct. Mater.*, 2017, **27**, 1604943.
17. C. Tang, L. Zhong, B. Zhang, H. Wang and Q. Zhang, *Adv. Mater.*, 2018, **30**, 1705110.
18. D. Su, S. Dou and G. Wang, *Adv. Energy Mater.*, 2015, **5**, 1401205.
19. Y. Liu, X. Wang, X. Song, Y. Dong, L. Yang, L. Wang, D. Jia, Z. Zhao and J. Qiu, *Carbon*, 2016, **109**, 461-471.
20. W. Ren, H. Zhang, C. Guan and C. Cheng, *Adv. Funct. Mater.*, 2017, **27**, 1702116.
21. D. Sun, D. Ye, P. Liu, Y. Tang, J. Guo, L. Wang and H. Wang, *Adv. Energy Mater.*, 2018, **8**, 1702383.
22. T. Wu, M. Jing, Y. Liu and X. Ji, *J. Mater. Chem A*, 2019, **7**, 6439-6449.
23. M. Hou, Y. Qiu, G. Yan, J. Wang, D. Zhan, X. Liu, J. Gao and L. Lai, *Nano Energy*, 2019, **62**, 299-309.
24. Y. Li, K. Chang, E. Shangguan, D. Guo, W. Zhou, Y. Hou, H. Tang, B. Li and Z. Chang, *Nanoscale*, 2019, **11**, 1887-1900.